ISBN: 978-3-95450-248-6 ISSN: 2673-5490 doi: 10.18429/JACoW-IPAC2025-THPM008

VIRTUAL TEMPERATURE MEASUREMENTS OF FERRITE IN IN-VACUUM KICKER MAGNETS

F. M. Velotti, P. A. Arrutia Sota, M. Diaz Zumel, G. Favia, F. Huhn, K. Ragkousis, P Trubacova
CERN, Geneva, Switzerland

Abstract

The Large Hadron Collider (LHC) Injector Upgrade project has achieved unprecedented beam brightness levels, to fulfill the High Luminosity LHC requirements. This higher intensity has introduced significant challenges for some of the Super Proton Synchrotron (SPS) kickers, specifically concerning beam-induced heating and vacuum rise due to electron cloud. The primary concern is the integrity of the ferrite within the kicker magnets, which is critical to the system's operation and availability. Currently, temperature monitoring relies on temperature probes (PT100) installed on the magnet's frame, but these do not provide direct measurements of ferrite temperature. To address this limitation, we present a proof of concept for a method using deep learning techniques to develop a virtual temperature sensor, enabling real-time monitoring of ferrite temperatures across the kicker module.

INTRODUCTION

The Super Proton Synchrotron (SPS), CERN's second-largest accelerator, relies on in-vacuum MKP kicker magnets to steer the injected beam onto its proper orbit. There are two families: MKP-S and MKP-L [1]. The MKP-S type has a smaller horizontal aperture and is primarily used to inject a 14 GeV beam for fixed-target physics, whereas the MKP-L type was installed to inject beams with energies up to 26 GeV for the LHC. For many years, the MKP-L was the principal intensity limitation for the SPS owing to its significant beam-coupling impedance [2]. A new version, installed in 2023, reduced this impedance considerably, so the MKP-S has now represents one of the main constraints for scrubbing.

The limitation arises from heating of the kicker system, specifically the ferrite, which can alter magnetic properties and, in extreme cases, lead to material failure. The only installed temperature sensor is mounted on the support structure, not on the ferrite itself (as this was not possible with a classic PT100), so the ferrite temperature cannot be measured directly.

To bridge this gap, we developed a DeepONet-based virtual sensor [3] that predicts the full temperature field of the kicker from the beam-power history. The ultimate goal is to protect the ferrite and kicker system from uncontrolled heating, enabling more efficient machine operation without unnecessary interlocks.

METHODS

Our objective is to develop a virtual sensor that can estimate ferrite temperature online. A crucial component is a high-quality surrogate model that can predict the temperature at any point within the model, given the beam-induced power and material properties. The workflow is as follows:

1. Generate a large data set of temperature fields with a finite-element solver by sampling multiple beam-power histories $P(t)$ and a range of values for the unknown material properties.
2. Train a DeepONet surrogate model to predict the temperature field given the beam power and the material properties.
3. Infer the unknown material properties using a Markov Chain Monte Carlo (MCMC) method based on the surrogate model and real temperature data from the installed PT100 sensor.

This results in a surrogate model capable of predicting the temperature field sufficiently fast for real-time application, at any point in the model from beam power and material properties.

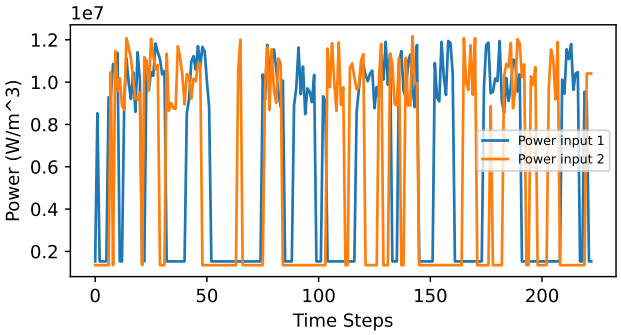

Figure 1: Example of a beam power history $P(t)$ used as input to the model.

Data Generation

As a proof of concept, we consider a simplified geometry: a cube composed of two materials, steel and aluminium. Heating is modelled as a line source embedded in the aluminium, with heat diffusion described by the following 3D partial differential equation (PDE):

$$\rho c\, \partial_t T = \nabla \cdot (k \nabla T) + Q(t), \tag{1}$$

where T is the temperature, ρ is the density, c is the specific heat capacity, k is the thermal conductivity, and $Q(t)$ represents the heat source.

The input term $Q(t)$ was randomly generated as a pulsed source to emulate the beam characteristics in a realistic SPS operational scenario. An example is shown in Fig. 1.

ISBN: 978-3-95450-248-6 ISSN: 2673-5490 doi: 10.18429/JACoW-IPAC2025-THPM008

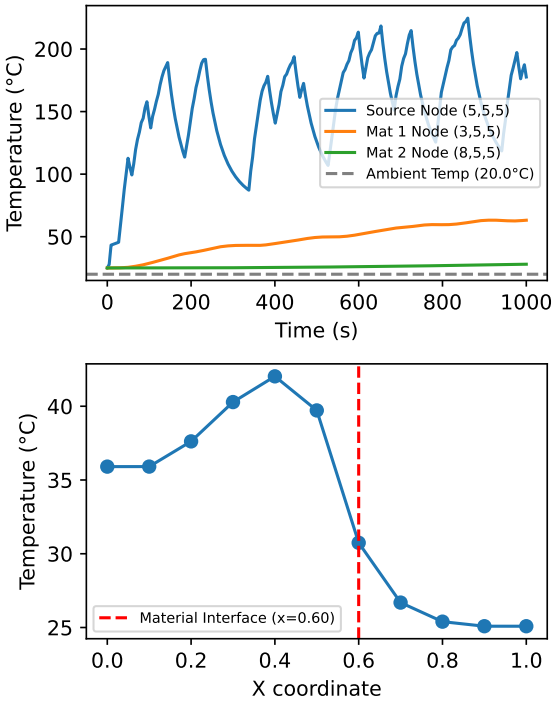

Figure 2: (top) Temperature evolution as a function of time at a specific point in space for the two materials (blue: source, orange: aluminium, green: steel). (bottom) Temperature distribution along the X coordinate at the final time step.

The resulting temperature evolution in both time and space for some selected cases is shown in Fig. 2.

The two material conductivities were scaled by two parameters $\alpha = (\alpha_1, \alpha_2)$. These parameters served as the unknowns for the estimation method. They serve chiefly to demonstrate feasibility.

Conditional DeepONet

Given a beam-power history $P(t)$ and material parameters $\alpha = (\alpha_1, \alpha_2)$, the goal is to approximate the nonlinear operator

$$\mathcal{G} : [P, \alpha] \mapsto T(\mathrm{x}, t, \alpha), \quad \mathrm{x} = (x, y, z), \tag{2}$$

where T solves Eq. (1) with piece-wise constant $k = \rho c \alpha$ and a line source $Q(t)$ centred on an arbitrary point.

DeepONet represents $\mathcal{G}$ as a sum of products of two neural subnetworks [3]:

$$\mathcal{G}(P)(\mathrm{s}) \approx \sum_{i=1}^{m} b_i(P)\, t_i(\mathrm{s}), \tag{3}$$

with *branch* outputs b_i depending solely on the global inputs P and *trunk* outputs t_i on the local coordinate vector. To include material dependence we extend the trunk inputs to $\mathrm{s} = (x, y, z, t, \alpha_1, \alpha_2) \in \mathbb{R}^6$. The trunk network is a function of the spatial coordinates and time, as well as of the unknown model parameters. As the input is a single point in space and time, the model will be able to predict the temperature field and any intermediate points of the training domain [3].

Each sub-network contains four fully connected layers with $[64, 128, 64, 32]$ neurons and uses ReLU activation. The loss is the mean-squared error between predicted and true temperatures. All inputs are normalised to $[0, 1]$ and outputs are standardised to zero mean and unit variance. Training uses the Adam optimiser with early stopping. Hyper-parameter tuning is deferred until real data become available.

Parameter Inference

The trained DeepONet surrogate is employed to infer the unknown thermal diffusivity scaling factors using Markov Chain Monte Carlo (MCMC) sampling. The DeepONet surrogate predicts the temperature at a specified spatial point over the entire time series. The MCMC method is used to get an estimation of the real posterior distribution of the model parameters, namely α_1 and α_2 via a maximum a-posteriori estimation and the possible noise on the data. In this case, it is used Slice-sampling [4] to explore the posterior distribution, assuming a uniform prior for the parameter(s) over the available domain $[0.6, 1.0]$. Throughout this process, the DeepONet is treated as a black-box function. The data utilized is the time-series temperature evolution of a model with $\alpha_1 = 0.7$ and $\alpha_2 = 0.7$ at an arbitrarily selected point in space, representing data obtainable from a temperature probe. This effectively allows for the inference of the model's true underlying parameters.

The advantage of this approach with respect to a classic error minimization between model prediction and data is that the MCMC method provides a posterior distribution of the parameters, allowing for a more robust estimation of the uncertainty, resilience to under constrained problems as well as their joint probability distribution.

RESULTS

The performance of the DeepONet-based virtual temperature sensor was evaluated using simulated data. Figure 3 visually compares the temperature distribution at the final time step as calculated by the Finite Element (FE) solver (ground truth) and predicted by the DeepONet surrogate. The color scale indicates temperature, showing a strong qualitative agreement between the true and predicted temperature fields, with the hottest regions accurately identified by the surrogate model.

Figure 4 presents the temporal evolution of temperature at a selected point in space, mimicking a PT100 sensor reading. The blue line represents the true temperature from the FE solver, while the orange line shows the DeepONet surrogate's prediction. The grey plot in the background depicts the input power P(t) applied to the system. The predicted temperature closely tracks the true temperature fluctuations over the entire time series, demonstrating the model's capability to capture the dynamic thermal response of the system to varying power inputs.

The parameter inference capability was tested using an MCMC method. Figure 5 displays the posterior probability

ISBN: 978-3-95450-248-6 ISSN: 2673-5490 doi: 10.18429/JACoW-IPAC2025-THPM008

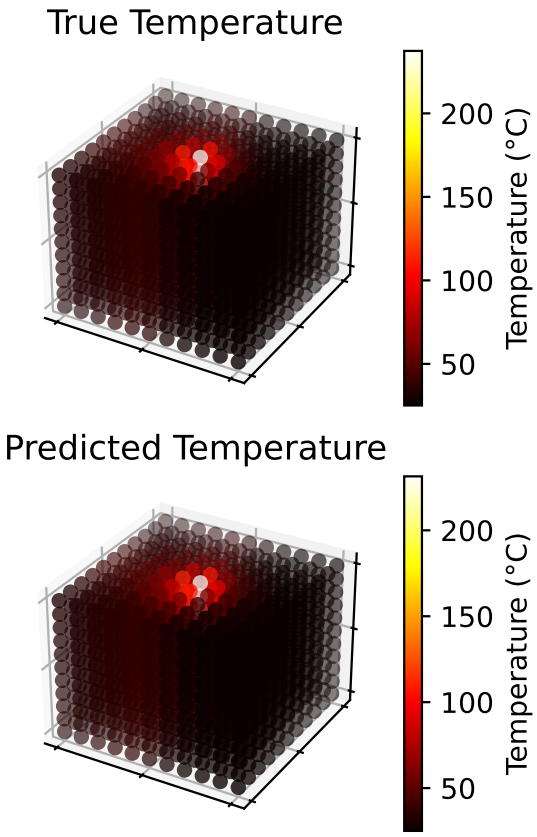

Figure 3: Temperature at the last time step as obtained from the FE solver (top) and the DeepONet surrogate (bottom). The color scale representing the temperature.

distributions for the two unknown thermal diffusivity scaling factors, α_1 and α_2. The distributions are sharply peaked around the true values (indicated by the red dashed line), which were used to generate the synthetic measurement data ($\alpha_1 = 0.7$ and $\alpha_2 = 0.7$). This result shows the model's ability to accurately infer material thermal properties from sparse temperature measurements for the case used as example. The validation of the method for multiple material properties and different unknowns will have to be analysed in detail.

DISCUSSION

Future work will address complex kicker geometry and extend the method toward hardware-design optimisation. Dependence on the initial and boundary temperatures will be included. For geometry optimisation, a more suitable DeepONet variant—such as that in [5]—will be investigated.

CONCLUSION

This proof-of-concept study demonstrates the feasibility of a virtual temperature sensor for ferrite monitoring in SPS MKP-S in-vacuum kicker magnets. A DeepONet surrogate, trained on FEM-generated data, predicts spatio-temporal temperature fields from the beam-power history and inferred

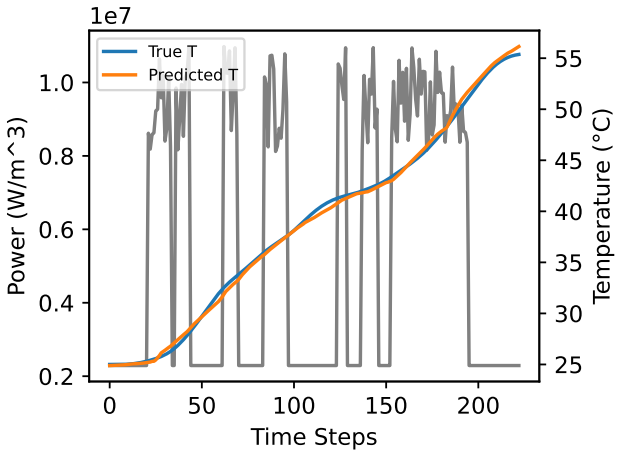

Figure 4: Temperature evolution for the selected point in space representing the PT100 sensor. The blue line is the real temperature from the FE solver and the orange line is the prediction from the DeepONet surrogate. On the left axis, the input power $P(t)$ for this specific case is plotted in grey.

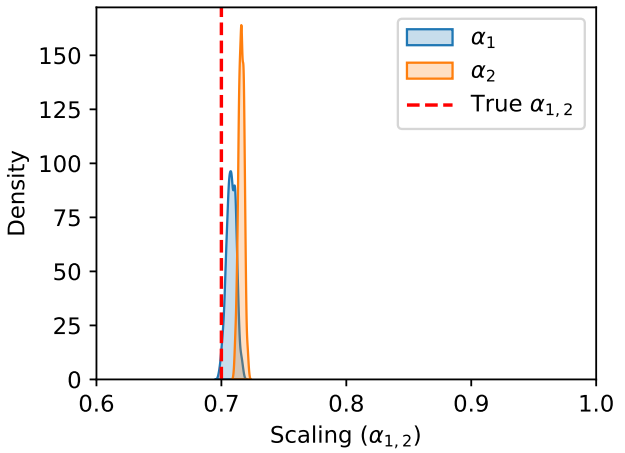

Figure 5: Posterior probability distribution of the two parameters α_1 and α_2 as obtained from the MCMC method. The red line is the true value of the parameters used to generate the data.

material properties. In simulation, the virtual sensor reproduces the overall temperature distribution and dynamic response at sensor locations. The integrated MCMC routine further shows that key thermal parameters can be recovered from sparse measurements, providing quantified uncertainty.

Although encouraging, these results rely entirely on simulated data and a simplified geometry; real-machine validation is therefore required. Future work will deploy and benchmark the methodology on the operational MKP-S kicker system, extend the model to the full 3-D geometry, and refine parameter inference using live beam and temperature data.

ISBN: 978-3-95450-248-6 ISSN: 2673-5490 doi: 10.18429/JACoW-IPAC2025-THPM008

REFERENCES

[1] G. Favia *et al.*, "SPS injection kicker system: 2023 operational experience and upgrade proposals for high-luminosity LHC", in *Proc. IPAC'24*, Nashville, TN, USA, 2024, pp. 1088–1091. doi:10.18429/JACoW-IPAC2024-TUPC38

[2] M. Barnes *et al.*, "Operational experience of a low beam coupling impedance injection kicker magnet for the CERN SPS ring", in *Proc. IPAC'23*, Venice, Italy, 2023, pp. 4352–4355. doi:10.18429/JACoW-IPAC2023-THPA164

[3] L. Lu, P. Jin, G. Pang, Z. Zhang, and G. E. Karniadakis, "Learning nonlinear operators via DeepONet based on the universal approximation theorem of operators", *Nat. Mach. Intell.*, vol. 3, no. 3, pp. 218–229, 2021. doi:10.1038/s42256-021-00302-5

[4] R. M. Neal, "Slice sampling", *arXiv:physics/0009028*, 2000. doi:10.48550/arXiv.physics/0009028

[5] J. He, S. Koric, D. Abueidda, A. Najafi, and I. Jasiuk, "Geom-deeponet: A point-cloud-based deep operator network for field predictions on 3d parameterized geometries", *Comput. Methods Appl. Mech. Eng.*, vol. 429, p. 117 130, 2024. doi:10.1016/j.cma.2024.117130